EFFECT OF DELAMINATION PROPAGATION ON MECHANICAL BEHAVIOR IN COMPRESSION AFTER IMPACT

Yuichiro Aoki*, Hiroshi Kondo ** and Hiroshi Hatta*
***Japan Aerospace Exploration Agency, Tokyo, Japan**
****** Tokai University, Kanagawa, Japan**

Keywords: *Delamination, CAI strength, Progressive failure analysis, fracture toughness*

Abstract

The aim of this study is to investigate the behavior until final failure of the composite laminates with artificial multiple delaminations under compression load. Three types of the CFRP laminates with embedded multiple artificial delaminations whose shapes imitate typical impact induced damages. The effect of the multiple delamination size and trough-the-thickness shape on failure behavior is examined by experiment and three-dimensional progressive failure analysis. The finite element model based on a fracture mechanics is used to simulate the growth of multiple delaminations under compression load. The experimental results are compared with the results obtained from the analyses. This study provides the information of the critical load which leads to structural instability of the CFRP laminates subjected to compression load. The critical load is highly correlated with delamination propagation and local buckling in delaminated region.

1 Introduction

The use of composite materials in the aerospace field has increased to achieve a weight reduction with a high strength and stiffness. Carbon fiber reinforced plastic (CFRP) laminates are used in a wide range of applications of aerospace structures. The structures made of composite laminates, however, are vulnerable to out-of-plane impact damages such as delaminations, transverse cracks and fiber breakage because they have no reinforcement through the thickness and material discontinuities between layers. The damages are barely visible from outside but cause reductions of stiffness and strength of the composite structures, especially compression after impact strength (CAI strength) is degraded significantly. For this reason, CAI strength is considered as one of the crucial factors in the aircraft design of composite primary structures and material screening for new composite systems. Therefore, deeper understanding in mechanics of CAI phenomenon must be indispensable to identify the dominant property of the residual strength in composite structures. Many researches on CAI phenomenon have conducted by a number of experiments and numerical analysis [1-8]. From these works, interesting nature of CAI behavior has been revealed, where the findings are divided into two phases: impact and compression behaviors. Impact-induced delamination is a crack which runs in the resin-rich area between layers of different fiber orientation and not between layers in the same orientation [8, 9]. Analytical methods are also required to clarify the damage accumulation problems in composite laminates. Various numerical methods have been proposed to study the mechanism of damage accumulation in composite laminates. The virtual crack closure technique (VCCT) has been successfully used to study the stability of delamination propagation under the assumptions of initial delaminated area and self-similar delamination growth [10, 11]. In order to simulate progressive delaminations, interface models based on damage mechanics have been proposed and developed [12, 13]. A cohesive crack model based on the Dugdale-Barenblatt cohesive zone approach has also been introduced. The mechanical response of the cohesive model is determined by traction and energy dissipation in the vicinity of a crack tip. The cohesive model is convenient and attractive for simulating the delamination propagation in composite laminates since the fracture interface can be prescribed. Various cohesive elements have been

developed and proposed for simulating the crack-like damage in composite materials [14-18].

Works on CAI behavior has revealed that the reduction in the CAI strength is dependent on the shape, area and position of the delamination. Increase of the G_{IIC} leads to obvious improvement of residual CAI strength since the mode II fracture toughness, G_{IIC}, correlates with the impact resistance [19, 20]. Impact-induced delamination growth in compression loaded composite laminates may cause final failure. Hence, the presence of impact damage and growth of a critical delamination must be considered to clarify the mechanism of CAI failure. Most investigations on delamination growth under compression load have been conducted by using composite laminates with impact-induced and artificially embedded delaminations, focusing on the correlation with local and global buckling [21-25]. From these investigations, the artificial delamination is reliable for validation of the analysis method developed for CAI simulation. However, the numerical analysis considering multiple delaminations growth in composite laminates under compression load, being very complicated, is still difficult because of combination of the local and global instabilities, both of which can be a trigger of the failure. The final failure mode with delamination propagation has not been well understood. Therefore, numerical investigation on compressive failure mechanism of composite laminates with multiple delaminations is still an active research topic to clarify the mechanism of CAI phenomenon.

The aim of this study is to investigate the behavior until final failure of the composite laminates with artificial multiple delaminations under compression load. Three types of the CFRP laminates with embedded artificial multiple delaminations whose shapes imitate typical impact induced damages. The effect of the multiple delamination size and trough-the-thickness shape on failure behavior is examined by experiment and three-dimensional progressive failure analysis. The finite element model based on the VCCT is used to simulate the growth of multiple delaminations under compression load. The experimental results are compared with the results obtained from the analyses. This study provides the information of the critical load which leads to structural instability of the CFRP laminates subjected to compression load. The critical load is highly correlated with delamination propagation and local buckling.

2 Experimental

2.1 Preparation of specimens

The material system used in this study was IM600/133 (Q-C133, Toho rayon), an intermediate modulus-high strength carbon fiber and 180 ℃ cure-type toughened epoxy resin system. This material is used for various aircraft structure because of a good CAI resistant property. A large amount of fundamental data for this material is obtained by the internet website of JAXA-ACDB: http://www.jaxa-acdb.com.

Figure 1 indicates a typical shape of accumulated delamination created by a drop weight impact of 6.7 J/mm in 32ply quasi-isotropic CAI specimen made from the same material system above. Each picture was taken by phased array type three-dimensional ultrasonic C-scanner. Fan-shape delamination is created between each interface and each fan-shape delamination rotates 45 degrees around the center of the specimen in a spiral manner. The rotation angle depends on fiber direction of the layers below and above delamination. Thus projected delamination area is circle and accumulated delamination shape through the thickness is likely a conical. Figure 2 (a) indicates a schematic view of the accumulated delamination structure taken from detail C-scan image. It is found that an equivarent configuration of the four fan-shape delaminations is one circle delamination as shown in Fig. 2 (b).

The stacking sequence of the test specimen with artificial multiple delamination was $[45/0/-35/90]_{4s}$. There were seven different circle multiple

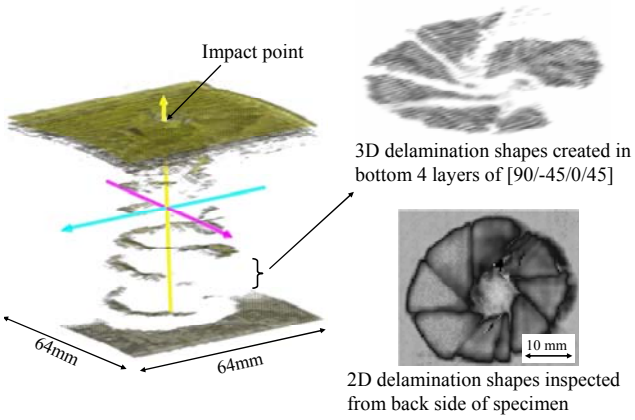

Fig. 1 Typical impact-induced delamination shape in 32ply IM600/133 quasi-isotropic laminates taken from three-dimensional ultrasonic scanner

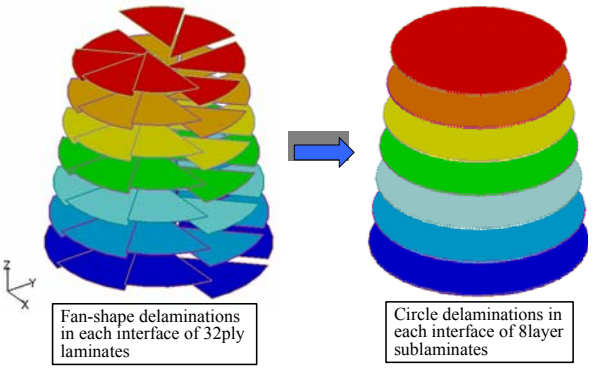

(a) Fan-shape (b) Circle

Fig.2 Simplification of multiple fan-shape delaminations

delaminations and the laminates was divided into eight sublaminates with a lay-up of [45/0/-45/90]. A pair of PTFE film with single thickness of 10 μm was laid between plies to form a artificial delamination. Specimens were manufactured with different size of delaminations through thickness direction. In every specimen, the delaminated area was a circular with diameter of D_i , which offered a equivalent shape of realistic impact-induced delamination shown as Fig. 3. There were three types of the specimen with artificial multiple delaminations to compare the CAI behavior. Configuration of the delamination diameter is summarized in Table 1. Specimen 1 has seven equal diameter delaminations. The delamination diameters change linearly from top surface of the laminate to bottom surface in specimen 2. The delamination closest to the bottom surface is much larger than other delaminations in specimen 3, which is known as hat-shape delamination [6]. Total area in the table means sum of each delamination area. The number of each specimen was five.

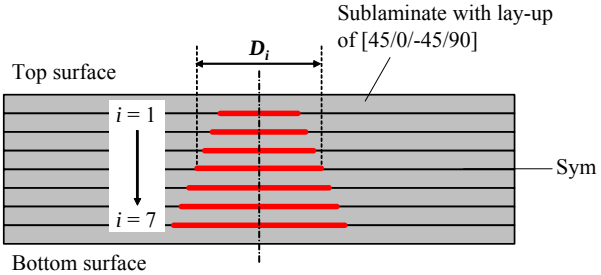

Fig.3 Lay-up of CFRP specimen and through-the-thickness positions of delamination

Table 1 Type of specimen

Diameter (mm)	Specimen 1	Specimen 2	Specimen 3
D_1	22	16	16
D_2	22	18	18
D_3	22	20	20
D_4	22	22	22
D_5	22	24	24
D_6	22	26	26
D_7	22	28	40
Total area (mm^2)	2659.6	2747.5	3388.1

The artificial delamination in the specimen 2 obtained by three-dimensional ultrasonic C-scanner is shown Fig. 4.

Each specimen was cut from the cured plate to the dimensions of 150 mm long by 100 mm wide in reference to the SACMA SRM 2R-94 as well as ASTM 7136/D. The average thicknes is 4.6 mm while the thickness at the center is 4.7mm due to embedded artificial delaminations.

2.2 Compression test

Compression tests were carried out at room temperature (23℃ ± 3℃) by a screw-driven test machine, INSTRON 1182. The compressive load was applied to the specimen under displacement control with a crosshead speed of 0.5 mm/min. CAI

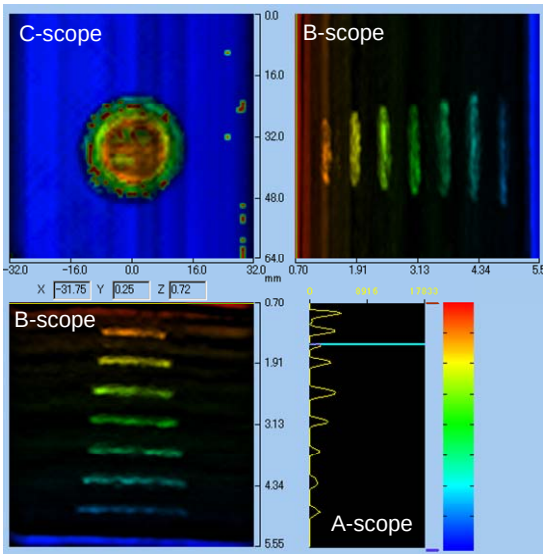

Fig.4 Ultrasonic C-scanning image of specimen 2 taken before test

test fixture described in the SACMA standard is used, which is designed to hold the specimen and out-of-plane displacement at side edges are simply supported by knife edge fixtures. Overview of the test is shown in Fig. 5. Deflections at the center of both surfaces were measured by laser displacement sensors (KEYENCE LK-080). The compression load, displacement, deflections and strains are measured by KYOWA PCD-300 data logger with a sampling rate of 20 Hz during the test.

3 Finite element analysis

A commercially available finite element analysis code, ABAQUS Ver.6.6, was used for the present analysis. The finite element model was constructed from layers of three-dimensional 8-node orthotropic brick composite elements. For modeling the specimen with multiple delaminations, two layers of elements were tied at the interface except for the delamination area. At the delaminated regions, contact conditions were applied to prevent interpenetration of the elements during analysis. Each delamination was given a small out-of-plane displacement as an initial imperfection to initiate buckling during the analysis. The maximum imperfection is 0.02 mm at the center of the specimen in reference to first buckling mode obtained by linear buckling analysis. The unidirectional linear elastic material properties shown in Table 2 were used for the present analysis considering the stacking direction. Delamination propagation under compression load was simulated by the added option of VCCT for ABAQUS Ver. 1.2.

A fracture criterion for delamination propagation is defined as following power law.

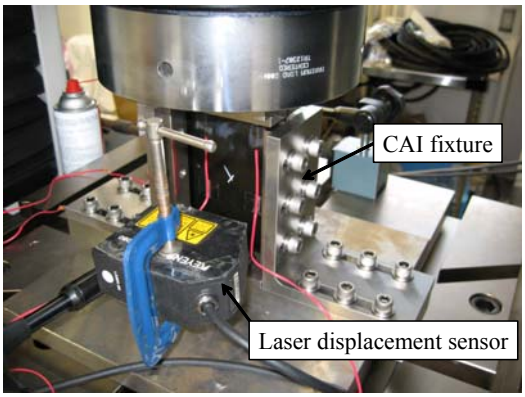

Fig.5 Compression test set-up by CAI fixture

$$\left(\frac{G_{\mathrm{I}}}{G_{\mathrm{I}c}}\right)^{am}+\left(\frac{G_{\mathrm{II}}}{G_{\mathrm{II}c}}\right)^{an}+\left(\frac{G_{\mathrm{III}}}{G_{\mathrm{III}c}}\right)^{ao}=1 \qquad (1)$$

where, $am = an = ao = 1$, and G_{Ic}, G_{IIc}, G_{IIIc} are fracture toughness for each separation mode shown in Table 2, where equal values of G_{IIc} and G_{IIIc} are used. In present analysis, effect of mode II fracture toughness on compressive behavior is also considered. A static non-linear analysis including geometrical nonlinearity was conducted to predict post buckling behavior of the specimens. Boundary conditions were used to represent the constraint provided by the experiment including knife-edge support at the side edges. Displacement was applied as a pressure loading over the nodes on element face normal to the loading direction. Finite element model is shown in Fig. 6.

4 Results and Discussions

4.1 Experimental results

CAI strength results for each specimen are shown in Fig. 7 with reference data of the specimen with realistic impact damage with energy of 6.7J/mm. Although the data shows some scatter bands, CAI strength of the specimen with artificial delaminations is relatively smaller than that of the laminates with realistic impact delamination. The average CAI strength for the specimens containing artificial delaminations was smaller than that for impacted specimens. CAI strength for specimen 3

Table 2 Material properties of IM600/133

Elastic Property	
E11	137 GPa
E22	8.2 GPa
E33	8.2 GPa
ν12	0.34
ν13	0.34
ν23	0.34
G12	4.36 GPa
G13	4.36 GPa
G23	3.0 GPa
Fracture property	
G_{Ic}	0.44 kJ/m^2
G_{IIc}	1.86 kJ/m^2
G_{IIIc}	1.86 kJ/m^2

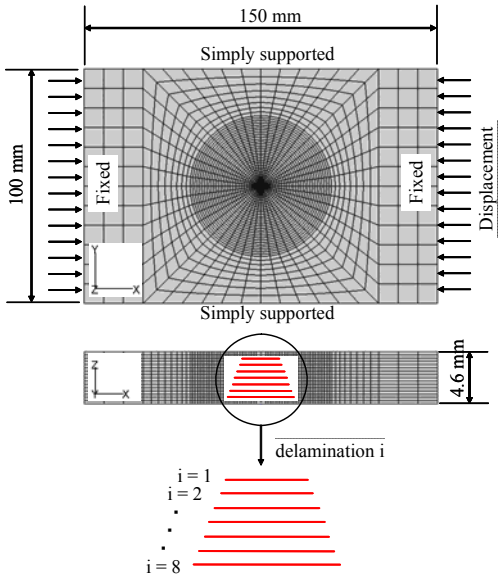

Fig. 6 Finite element model with multiple delaminations

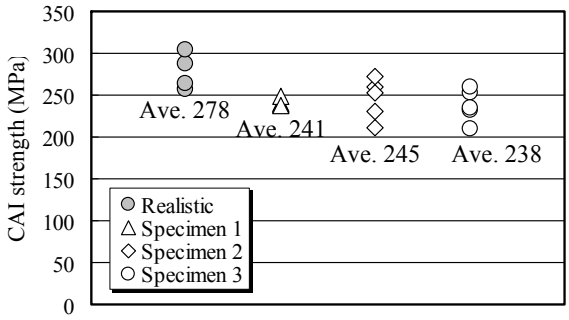

Fig. 7 Results of CAI strength for each specimen

was relatively smaller than other specimens, which was caused by larger total area of delaminations.

Deformation of the bottom surface of specimen 2 was shown in Fig.8 with load and out-of-plane displacement measured by laser displacement sensor. It was found that out-of-plane displacement did not increase until a load of about 97 kN while sudden increase occurred at a load of 97.5 kN. The top and bottom surfaces displaced in opposite directions. This sudden buckling event is believed to be caused by rapid delamination propagation in the specimen. The same behavior was seen in the case of specimen 1 and 3. The top and bottom surface displacement were the very small until a sudden separation at a maximum load. Since this material has high interlaminar fracture toughness, thus the final failure

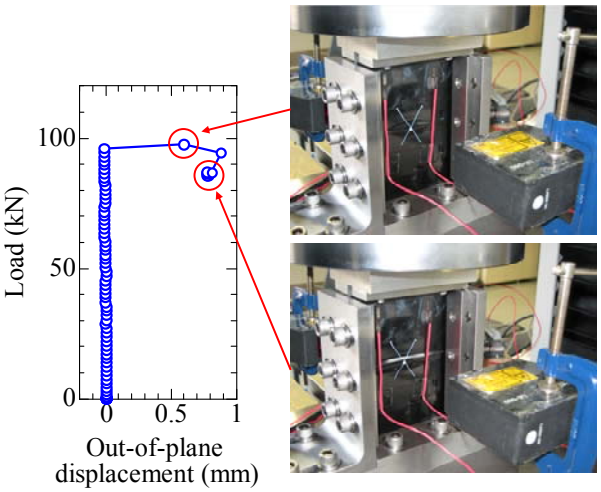

Fig. 8 Out-of-plane displacement for specimen 2

mode of the specimen was catastrophic collapse with sudden delamination propagation. Ultrasonic C-scan images of failed specimens taken from the bottom surface are shown in Fig. 9. The delamination spread in the transverse direction in all cases while the band width of the delamination propagation was dependent on the initial delamination shape. The largest delaminations near bottom surface in specimen 2 and 3 was not thought to be a direct trigger of the delamination growth because the circle shape still remained after final failure. The instability of other delaminations was thought to be the trigger for final failure, with delaminations having spread in the transverse direction.

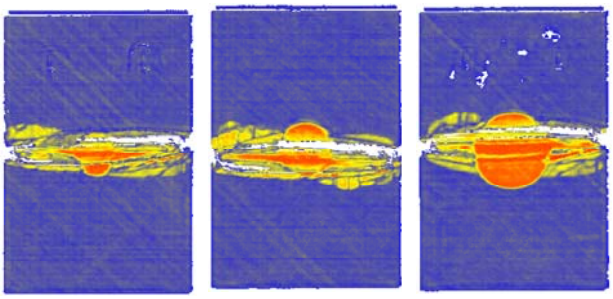

(a) specimen 1 (b) specimen 2 (c) specimen 3

Fig. 9 Ultrasonic C-scanning images taken after the compression tests

4.2 Analysis results

The analyses were difficult to carry out due to stability and convergence problems for the complete behavior until the final failure. Present analysis is sill preliminary stage and only the effect of fracture toughness on the initiation of delamination

propagation which leads to instability of laminates. The specimen 2, containing the multiple delaminations whose diameters change linearly from top to bottom surface, was selected as a base model to conduct the analysis. In this analysis, fracture toughness is selected as shown in Table 3.

Compressive behaviors of delaminated laminates are well understood from the relationship between the applied load and the center deflections of the back surfaces shown as Fig. 10. Local buckling at the delaminated portion was dominant deformation mode for all models. In this figure, delamination threshold is indicated by symbols and compressive behavior of an intact plate is plotted as a reference. Some analyses had not been completed because the analysis could not converge at a final increment, where delamination propagation and deformation of laminates became significant and the system became rather unstable. From this figure, buckling and delamination threshold loads of delaminated laminates increased linearly with the mode II fracture toughness increase. Predicted delamination propagations at the final load level of 348 kN for model A are shown in Fig. 11. The largest delamination closest to the bottom surface tends to remain circular while other delaminations spread in the transverse direction. This point can explain the characteristics of the damage propagation mentioned in the experimental results.

Table 3 Fracture toughness for each model

Model	G_{Ic} (kJ/m^2)	$G_{IIc} = G_{IIIc}$ (kJ/m^2)
A (Base model)	0.44	1.86
B	0.44	0.2325
C	0.44	0.465
D	0.44	3.72
E	0.11	1.86

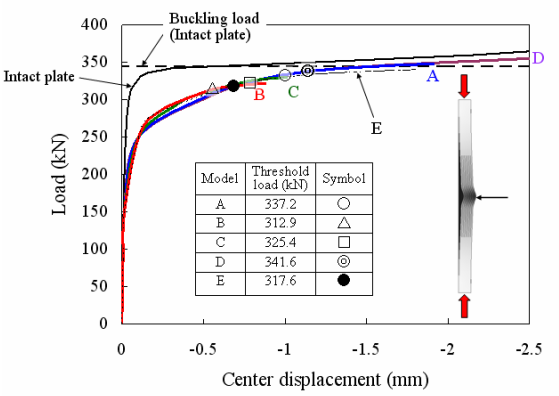

Fig. 10 Relationship between the applied load and center deflections of the back surfaces

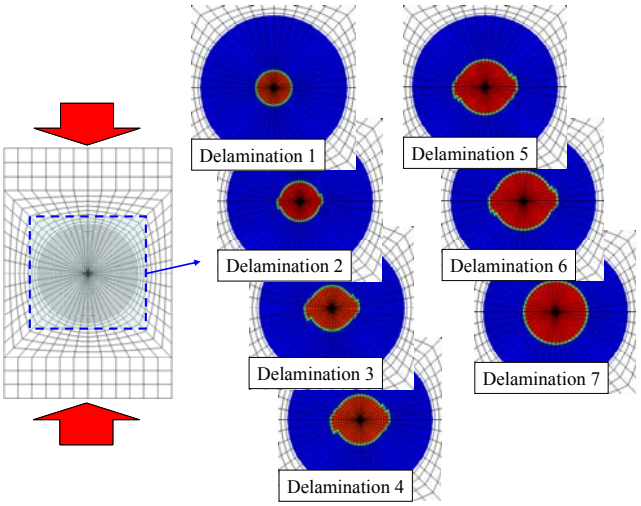

Fig. 11 Predicted delamination shapes for model A at the load level of 343 kN

References

[1] Richardson M. O. W. and Wisheart M. J., Review of low velocity impact properties of composite materials, *Composites A*, Vol. 27, pp.1123-1131, 1996.

[2] Guédra-Degeorges D., Recent advances to assess mono- and multi-delaminations behaviour of aerospace composites, *Composites Science and Technology*, Vol. 66, pp.796–806, 2006.

[3] Freitas M. de. and Reis L., Failure mechanisms on composite specimens subjected to compression after impact, *Composite Structures*, Vol. 42, pp 365-373, 1998.

[4] Hichen S. A. and Kemp R. M. J., The Effect of Stacking Sequence on Impact Damage in a Carbon Fiber/Epoxy Composite, *Composites*, Vol. 26, pp. 207-214, 1995.

[5] Shyr T.-W. and Pan Y.-H., Impact resistance and damage characteristics of composite laminates, *Composite Structures*, Vol. 62, No. 2, pp. 193-203, 2003.

[6] Ishikawa T., Sugimoto S., Matsushima M. and Hayashi Y., Some Experimental Findings in CAI Tests of CF/PEEK and Conventional CF/EPOXY Flat Plates, *Composites Science and Technology*, Vol. 55, pp. 349-362, 1995.

[7] Dost E. F., Ilcewicz L. B., and Avery W. B., The Effects of Stacking Sequence on Impact Damage Resistance and Residual Strength for Quasi-isotropic Laminates, *ASTM STP*, 1110, pp. 476-500, 1991.

[8] Wu H. Y. T. and Springer G. S., Measurements of Matrix Cracking and Delamination Caused by Impact on Composite Plates, *Journal of Composite Materials*, Vol. 22, No. 6, pp. 518-532, 1988.

[9] Cui W. and Wisnom M. R., A Combined Stress-Based and Fracture-Mechanics-Based Model for Predicting Delamination in Composites, *Composites*, Vol. 24, pp. 467-474, 1993.

[10] Razi H. and Kobayashi A. S., Delamination in cross-ply laminated composite subjected to low-velocity impact, *AIAA Journal*, Vol. 31, No. 8, pp. 1498-1502, 1993.

[11] Liu S. and Chang F. K., Matrix Cracking Effect on Delamination Growth in Composite Laminates Induced by a Spherical Indenter, *Journal of Composite Materials*, Vol. 28, 10, 940-977 (1994).

[12] Allix O. and Ladevèze P., Damage Analysis of Interlaminar Fracture Specimens, *Journal of Composite Materials*, Vol. 31, pp. 61-74, 1995.

[13] Mi Y., Crisfield M. A., Davies G. A. O. and Hellweg H. B., Progressive Delamination Using Interface Elements, *Journal of Composite Materials*, Vol. 32, pp. 1246-1273, 1998.

[14] Alfano C. and Crisfield M. A., Finite Element Interface Models for the Delamination Analysis of Laminated Composites: Mechanical and Computational Issues, *International Journal for Numerical Methods in Engineering*, Vol. 50, pp. 1701-1736, 2001.

[15] Borg R., Nilsson L. and Simonsson K., Modeling of Delamination using a Discredited Cohesive Zone and Damage Formulation, *Composites Science and Technology*, Vol. 62, pp. 1299-1314, 2002.

[16] Goyal V. K., Johnson E. R., Davila C. G. and Jaunky N., An Irreversible Constitutive Law for Modeling The Delamination Process using Interface Elements, *Proceedings of 43rd AIAA/ASME/ASCE/AHS/ASC Structures, Structural Dynamics, and Materials Conference*, Denver, Colorado, 2002.

[17] Aoki Y. and Suemasu H., Damage Analysis in Composite Laminates by using Interface Element, *Advanced Composite Materials*, Vol. 12, No. 1, pp. 13-22, 2003.

[18] Aoki Y., Suemasu H. and Ishikawa T., Damage propagation in CFRP Laminates subjected to low velocity impact and static indentation, *Advanced Composite Materials*, Vol. 16, No. 1, pp. 45-61, 2007.

[19] Masters J. E., Correlation of Impact and Delamination Resistance in Interleafed Laminates, *Proceedings of ICCM VI & ECCM2*, London, 3:96, 1987.

[20] Chou, I, Namba, K., Correlation of Damage Resistance under Low Velocity Impact and Mode II Interlaminar Fracture Toughness in CFRP Laminates, *Advanced Composite Materials*, Vol. 8, No. 2, pp. 167-176, 1999.

[21] Suemasu H, Kumagai T, Gozu K., Compressive behavior of multiply delaminated composite laminates. Part I: experiment and analytical development, *AIAA Journal*, Vol. 36, pp.1279–85, 1998.

[22] Suemasu H, Kumagai T., Compressive behavior of multiply delaminated composite laminates. Part II: finite element analysis, , *AIAA Journal*, Vol. 36, pp. 1286–90, 1998.

[23] Kyoung W-M, Kim C-G, Hong C-S, Buckling and postbuckling behavior of composite cross-ply laminates with multiple delaminations, *Composite Structures*, Vol. 43, pp. 257–74, 1999.

[24] Hwang S-F, Liu G-H., Buckling behavior of composite laminates with multiple delaminations under uniaxial compression, *Composite Structures*, Vol. 53, pp. 235–43, 2001.

[25] Wang X. W., Pont-Lezica I., Harris J. M., Guild F. J., Pavier M. J., Compressive failure of composite laminates containing multiple delaminations, *Composites Science and Technology*, Vol. 65, pp. 191–200, 2005.